IEEE Access
Multidisciplinary | Rapid Review | Open Access Journal

Received January 25, 2019, accepted March 2, 2019, date of publication March 8, 2019, date of current version March 26, 2019.

Digital Object Identifier 10.1109/ACCESS.2019.2903889

Optimum Methods of Thermal-Fluid Numerical Simulation for Switchgear

JIANGJUN RUAN[1], YONGCONG WU[1], PENG LI[2], MINGYANG LONG[1], AND YUJIA GONG[1]
[1]School of Electrical Engineering and Automation, Wuhan University, Hubei 430072, China
[2]College of Electrical Engineering and New Energy, China Three Gorges University, Yichang 443002, China

Corresponding author: Yongcong Wu (e-mail: 362121393@qq.com)

This work was supported by Natural Science Foundation of Hubei Province (2018CFB145).

ABSTRACT Thermal-fluid coupled calculation is an effective way to simulate the temperature rise and heat dissipation process of switchgear. But there are still problems such as huge calculation and low accuracy need to be solved. This paper discusses the optimization methods of the thermal-fluid coupled field for the switchgear from grid controlling, boundary conditions, and heat source calculation. First, the mesh adaption method based on posterior error estimation is proposed to achieve efficient mesh refinement with less redundancy. The final mesh size is only 32.3% of that obtained with the traditional global-refining method. Then, an external flow model is built to obtain the convective heat transfer coefficient of the enclosure, replacing the process of artificial choosing. The results show that the convective heat transfer coefficient at the enclosure under natural convection is 0.4 W/(m^2 ·° C) ∼1.4 W/(m^2·°C). Afterwards the eddy current field is used to solve the heat generation in the switchgear. The heat sources are coupled to the thermal-fluid calculation so that the influence of current non-uniformity, contact heat, and eddy loss is considered. At last, the methods are applied to the steady-state temperature rise simulation of KYN28A-12kV/630A switchgear and the results are compared with the test data. The maximum relative error between simulation and experimental results is 3.43%, which proves the validity of the mentioned methods.

INDEX TERMS Convective heat transfer coefficient, posterior error estimation, switchgear, thermal-fluid coupled simulation.

I. INTRODUCTION

Thermal field numerical calculation is an effect way to study the temperature rise and heat dissipation regularities in switchgear. It can provide data support for fault analysis, overheat monitoring, and cooling optimization. At present, solid heat conduction (HC) models and computational fluid dynamics (CFD) models are the most widely used. HC models are established upon the Fourier's Law with the advantages of low computation cost and good convergence [1], [2]. But the HC models cannot reflect the convective heat transfer process in switchgear, ignoring the local difference of airflow and heat exchange. CFD models solve the mass conservation equation, the momentum conservation equation, and the energy conservation equation to describe the state and energy change of gas in the switchgear. They can better rebuild the heat generation and dissipation process in switchgear. Li *et al.* [3] analyze the thermal field and flow field of 40.5kV gas-insulated switchgear and the influence factors are discussed. In [4], the comparison between natural convection and forced convection in the switchgear is carried out and the heat dissipation structure is optimized. Reference [5] study the impact of heat source location on the cooling condition of switchgear, providing supplementary guidance for the IEC TR 60890. Reference [6] tests the patterns of inlet/out let locations numerically to increase the heat dissipation rate of switchgear.

Airflow in switchgear contains various vortices and there is large velocity and temperature gradient near solid surfaces due to viscous force [7]. It is always time-consuming and tedious to predict the flow characteristics and to establish an appropriate mesh. In addition, the selection of model data may lead to obvious different results. So some scholars pay more attention to the discussion of key parameters and submodels in recent years. A. Sharma *et al.* [8] analyze the sensitivity of internal Nusselt number, Prandtl number, and

The associate editor coordinating the review of this manuscript and approving it for publication was Gang Mei.

Rayleigh number to the convective heat transfer coefficient (HTC). Lauriat and Desrayaud [9] reveals the important influence of surface radiation on conjugate natural convection. Bedkowski *et al.* [10] have done a great deal of researches on the improvement of thermal-fluid calculation in switchgear. They introduce the cutcell method and non-conformal mesh to reduce the mesh size. Besides, the selection of turbulence models, emissivity, and joint electric resistivity is optimized synthetically in [11], reducing the temperature difference from 12.5 °C to 8.1 °C. Electromagnetic-thermal-fluid coupled field is introduced in [12] to consider the strengthening effect of eddy current on thermal field. However, there is still room in improving the calculation accuracy and efficiency. The redundancy and inefficiency of mesh generation as well as the determination of model parameters in an actual industrial switchgear should be further optimized.

This paper focuses on the optimization methods of thermal-fluid numerical calculation for switchgear. Three aspects are mainly discussed: mesh control, boundary conditions, and heat sources. Firstly, mesh adaption based on posterior error estimation is applied to achieve effective mesh refining. Then, an external flow model is built to determine the convective HTC of the enclosure under different natural convection and forced convection environment. At last, heat sources in each components are solved by eddy current field and electromagnetic-thermal-fluid coupled calculation is used to analyze the influence of different heat sources. The proposed methods and obtained reference results are helpful to the improvement of the efficiency and accuracy in thermal-fluid numerical calculation for switchgear.

II. BASIC THEORY OF THERMAL-FLUID COUPLED CALCULATION

A. GOVERNING EQUATIONS

The general form of governing equation for thermal-fluid field is

$$\frac{\partial}{\partial t}(\rho\Phi) + \nabla\cdot(\rho v\Phi) = \nabla\cdot(\Gamma_\Phi\nabla\Phi) + S_\Phi. \tag{1}$$

where ρ is the gas density; Φ is the general variable of freedoms; $\boldsymbol{v}$is the velocity vector; Γ_Φ is the diffusion coefficient for freedom Φ; S_Φ is the source term.

The steady state of mass conservation equation, momentum conservation equation, and energy conservation equation are as in (2) $\sim$ (4) when taking $\Phi = 1$, $\Phi = v_\mathrm{i}$, and $\Phi = h$ respectively [3].

$$\nabla\cdot(\rho v) = 0 \tag{2}$$

$$\nabla\cdot(\rho v_\mathrm{i} v) = \nabla\cdot(\mu\nabla v_\mathrm{i}) + S_\mathrm{i} \tag{3}$$

$$\nabla\cdot(\rho h v) = \nabla\cdot(\frac{\lambda}{c_\mathrm{p}}\nabla h) + q_\eta + Q \tag{4}$$

where v_i is the component of velocity vector $\boldsymbol{v}$ in direction i (i represents direction x, y, and z); S_i is the momentum source term in direction i; h is the specific enthalpy; μ is the dynamic viscosity; c_p is the specific heat capacity; λ is the thermal conductivity; q_n is the viscous dissipation; Q is the heat source.

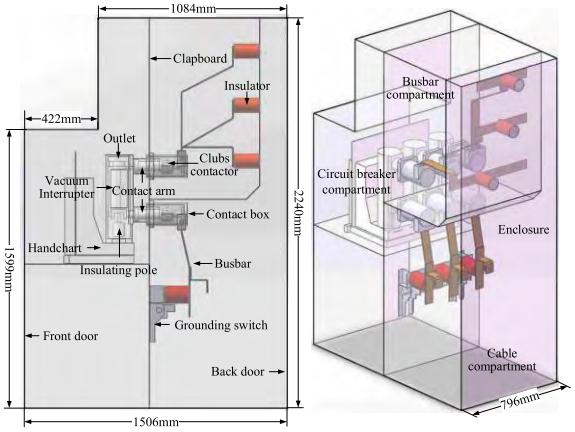

FIGURE 1. Simulation model of KYN28A-12kV/630A switchgear.

Specific enthalpy h is the total heat in a unit mass and the gas density ρ follows the ideal gas equation (6).

$$h = U + \frac{P}{\rho} = \frac{k}{2M}RT + \frac{P}{\rho} \tag{5}$$

$$PM = \rho RT \tag{6}$$

where U is the internal energy in a unit mass of material; R is the ideal gas constant; T is the temperature; M is the average molar mass; P is the pressure.

B. THERMAL-FLUID SIMULATION MODEL OF SWITCHGEAR

The simulation and discussion in this paper is based on the KYN28A-12kV/630A switchgear. Its structure is shown in Fig.1. The material of enclosure and clapboards is Al-Zn coated steel with thickness of 2mm. Current transformers, cables, and secondary equipments are removed both in the simulation model and the test sample to simplify the calculation. Besides, the low voltage compartment is not modeled considering the independence of its airflow.

C. BOUNDARY CONDITIONS

The truncated boundary of the simulation model in Fig.1 is located at the enclosure. Heat flux q_w induced by external convection can be described by (7) according to the third thermal boundary condition [13].

$$q_\mathrm{w} = h_\mathrm{c}(T_w - T_c) \tag{7}$$

where h_c is the convective heat transfer coefficient (HTC); T_w is the outer temperature of the enclosure; T_c is the ambient temperature.

Referring to the Stefan-Boltzmann Law, the radiative heat flux q_r between cavity and its inner wall is

$$q_\mathrm{r} = \frac{A_1(\sigma_\mathrm{b}T_1^4 - \sigma_\mathrm{b}T_2^4)}{\frac{1}{\varepsilon_1} + \frac{A_1}{A_2}(\frac{1}{\varepsilon_2} - 1)}. \tag{8}$$

where σ_b is the Stefan-Boltzmann Constant, 5.67×10^{-8} W/(m^2 · °C4); T_1 and T_2 are the temperature of inner wall and cavity respectively; ε_1 and ε_2 are the corresponding emissivity; A_1 and A_2 are their area.

Taking the environment as the cavity and the switchgear enclosure as the inner wall, the radiative heat flux q_r is as in (9) while $A_2 >> A_1$.

$$q_r = \varepsilon_1 \sigma_b (T_w^4 - T_c^4) \tag{9}$$

With (7) (9), the thermal boundary condition is

$$q_t = q_w + q_r = h_c(T_w - T_c) + \varepsilon_1 \sigma_b (T_w^4 - T_c^4). \tag{10}$$

where q_t is the total heat flux at the switchgear enclosure.

D. INFLUENCE FACTORS OF CALCULATION ACCURACY

Factors influencing the efficiency and accuracy of thermal-fluid calculation in switchgear include:

a. Mesh establishment: global refining is the most commonly used method to achieve mesh independence. However, the method is not applicable to complex 3D models due to the explosive growth of the mesh size. In addition, redundancy caused by excessive refinement may lead to large rounding errors.

b. Boundary condition: the empirical formulas for convective HTC h_c are [14]

$$N_u = 0.59 R_a^{0.25} \tag{11}$$

$$R_a = G_r \cdot P_r = \frac{g\beta\theta L^3}{(\mu/\rho)^2} \cdot \frac{\mu c_p}{\lambda} \tag{12}$$

$$h_c = \frac{\lambda N_u}{L}. \tag{13}$$

where N_u is the Nusselt number; R_a is the Rayleigh number; g is the gravitational acceleration; L is the characteristic length; β is the volume expansion coefficient; θ is the temperature difference between fluid and the solid surface.

In (11) ∼ (13), convective HTC h_c is the function of characteristic parameters of the external flow. However, it's still difficult to determine h_c as θ and L are often unknown in practical situation. Empirical values are always taken instead.

c. Heat source: Internal natural convection of switchgear is buoyancy forced airflow in limited space. Momentum source term S_i in (3) is closely related to the distribution of heat source Q. Electric contacts and Joule losses are main heat sources in switchgear. Besides, the proximity effect and skin effect as well as the eddy losses in the enclosure and clapboards should be further considered.

We will propose optimization methods in view of the mentioned three points in section III ∼ section V.

III. MESH ADAPTION BASED ON POSTERIOR ERROR ESTIMATION

Posterior error estimation refers to the process that estimates the error distribution in the numerical model based on the results of previous calculation and guides the mesh adaption.

At first, an initial mesh that reflects the basic characteristics of the thermal field and fluid field should be built so that the errors are correctly estimated. Then, mesh refinement is carried out according to the error distribution: elements with larger error are refined while the ones with smaller error remain unchanged. So the refinement process is more purposeful and the number of element is controlled.

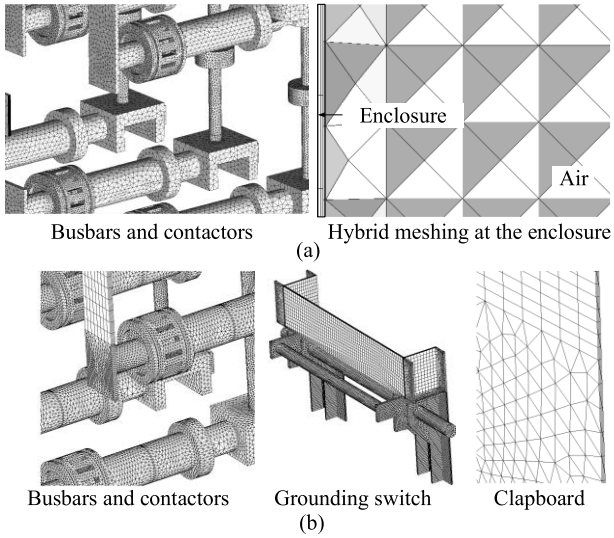

FIGURE 2. Hybrid mesh for switchgear. (a) Initial mesh for thermal-fluid field. (b) Mesh for eddy current field.

A. ESTABLISHMENT OF INITIAL MESH

Though there is still no uniform standard for the establishment of initial mesh, some references can still be found according to the features of the geometric structure and the internal airflow in switchgear.

1) HYBRID MESHING FOR THIN WALL STRUCTURE

The enclosure and clapboards of switchgear are thin wall structures with thickness of millimeter scale. Free mesh with tetrahedral elements may produce millions or even tens of millions of elements on the premise of good mesh quality. Mapping mesh with hexahedral elements is more suitable for these structures due to their geometric similarity. However, partial refinement is difficult to carry out in mapping mesh as the mapping relationship of element edges should be maintained. Then, the two mesh methods are combined to build the initial mesh here. Regular parts are meshed with hexahedral elements while the irregular and transitional zones are free meshed so that the advantages of small mesh size and mesh modifiability are combined.

The initial mesh for thermal-fluid calculation is shown in Fig.2. The mesh size in the thickness direction is 0.5mm and the amount of enclosure elements is 56832. Likewise, the mesh method is also applied to the eddy current calculation in section V. The meshing size in the thickness direction is 0.1mm and the amount of enclosure elements is 734400.

2) ELEMENT SIZE FOR THE BOUNDARY LAYER

There is a thin layer near the solid surfaces in which the velocity gradient is large. The calculation accuracy of the boundary layer have great influence on the thermal field. Parameter y^+ is the dimensionless distance of the boundary layer nodes which is defined by (14) (15). The requirement of y^+ varies as different algorithms are used [15].

$$y^+ = \frac{\rho \Delta y u_\tau}{\mu} \tag{14}$$

$$u_\tau = \left(\frac{\tau_\omega}{\rho}\right)^{1/2} \tag{15}$$

where y is the practical distance from the solid surface to the nearest element node; u_τ is the wall shear stress velocity; τ_ω is the wall shear stress.

The DNS method is to solve the governing equation (2) $\sim$ (4) in the boundary layer directly. It requires that the first node away from the solid surface is placed at the viscous sublayer where $y^+ < 1$ so that the structure of the boundary layer flow is simulated. In comparison, the wall function method establishes the relationship between the solid surface and the turbulent region with a set of semi-empirical formulas to simplify the simulation. It is often used in flow with high Reynolds number ($R_e > 10^5$) and requires that the nearest node is located at the logarithmic region where $y^+ = 30 \sim 60$.

Fig.3 shows the Reynolds number and wall shear stress distribution under normal working condition in switchgear. Results show that natural convection in switchgear belongs to low Reynolds number flow which means that the fluid viscous force plays an important role in the convection. Taking the area weighted average wall sheer stress $\tau_\omega = 1.4 \times 10^{-3}$ Pa, the practical distance Δy that satisfies $y^+ = 30 \sim 60$ is $\Delta y = 1.3 \sim 2.6$ cm and the one that satisfies $y^+ < 1$ is $\Delta y < 0.4$ mm.Considering that the generation of centimeter-scale elements on the millimeter-scale meshed busbar surface may cause serious distortion and ill-conditioned matrix, DNS method is more suitable for the solution of boundary layer flow in the internal natural convection of switchgear. So the suggested boundary layer mesh size of initial mesh is $\Delta y < 0.4$mm and the DNS method should be used.

B. MESH ADAPTION

1) POSTERIOR ERROR

Taking the finite volume method (FVM) as an example, the definition of posterior error is illustrated. The steady-state internal conservation form of (1) in a control volume V_{cell} is as in (16), in which the volume integral of V_{cell} is transferred into integral at boundary a and b in Fig.4. The values of a and b are calculated by interpolation with the adjacent nodes D and E, E and F respectively. Actually, numerical error results from the difference between the assumed distribution of freedom Φ which is described by interpolation and the actual field in

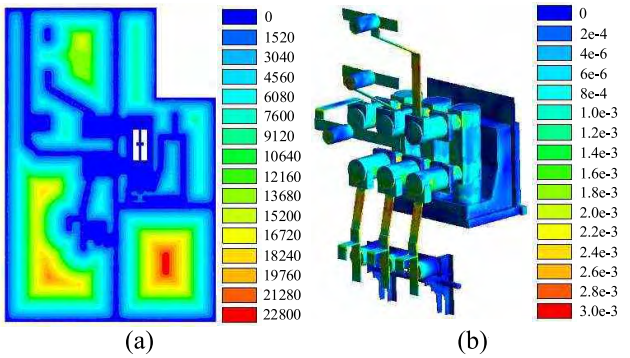

FIGURE 3. Feature parameters of natural convection in switchgear. (a) Reynolds number. (b) Wall shear stress(Pa).

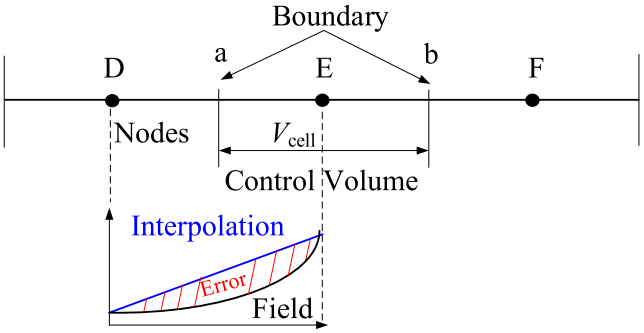

FIGURE 4. Gird meshing for finite volume method.

control volumes.

$$\int_V \boldsymbol{n} \cdot (\rho v \Phi) dA = \int_V \boldsymbol{n} \cdot (\Gamma_\Phi \nabla \Phi) dA + \int_V S_\Phi dV \tag{16}$$

Assuming that the numerical error is proportional to the nonlinearity of freedom Φ [16], the posterior error index can be defined as (17). Item$^2\Phi$ represents the degree of nonlinearity of Φ and $V_{\text{cell}}^{r/2}$ is the size coefficient of each control volume, taking the influence of volume size on interpolation error into consideration.

$$|e_i| = (V_{\text{cell}})^{\frac{r}{2}} \left|\nabla^2 \Phi\right| \tag{17}$$

where $|e_i|$ is the posterior error index; r is the volume weight, which is used to adjust the influence degree of the volume size.

It should be noted that $|e_i|$ is not the actual error between the simulation result and the true value, but only the estimation of the relative error distribution. $|e_i|$ can be further scaled as:

$$|e_i|_n = \frac{|e_i|}{|e_i|_{\max}}. \tag{18}$$

where $|e_i|_{\max}$ is the maximum posterior error index in the solution domain.

Calculation should be first carried out on the previous mesh to predict the error distribution of freedom Φ as $|e_i|_n$ are unknown. So, the error index is described as ''posterior''.

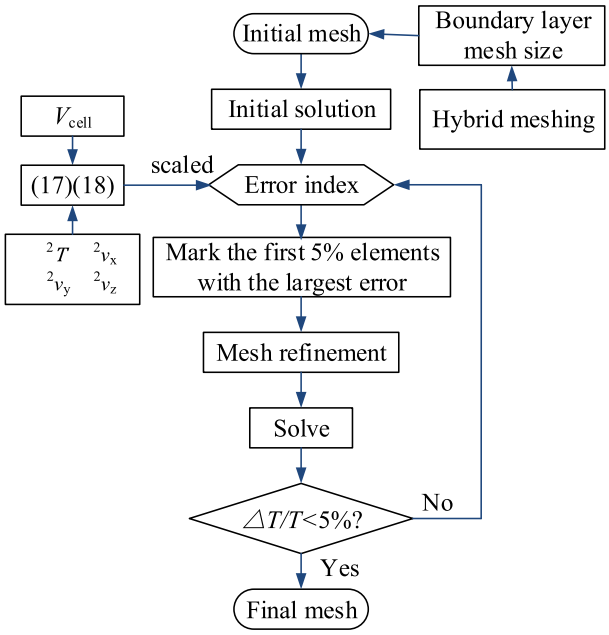

FIGURE 5. Flowchart of mesh adaption based on posterior error estimation.

2) MESH ADAPTION PROCESS

Simulation and mesh refinement are carried out alternatively based on the posterior error until the results converge. The flowchart is shown in Fig.5.

In order to prevent the rapid growth of mesh size, the first 5% elements with the largest posterior error index are refined in each mesh adaption. The convergence criterion is 5% of the maximum temperature.

3) MESH ADAPTION RESULTS OF THERMAL-FLUIDC CALCULATION IN SWITCHGEAR

According to section B.1, the error index distribution of the initial mesh (Fig.2 (a)) is shown in Fig.6. The volume weight is $r = 1$ and the observation plane is placed at the middle section of the switchgear.

In the initial mesh, the elements with large temperature error are mainly located near the enclosure and the clapboards, indicating the intense conjugate heat transfer near solid parts. The temperature error index is not large in the transitional fluid zones surrounding the current-carrying part, although there is strong heat exchange. Because the small mesh size of handcart, grounding switch, and busbar limits the element size V_{cell} in (17), maintaining the geometric consistency between the geometric model and the mesh. Likewise, the distribution of velocity error index mainly concentrates near solid surfaces and in narrow regions where the airflow is more complicated with large velocity gradient.

To further control the number of elements, mesh adaption is firstly carried out according to the velocity error index which is more concentrative in distribution. The final mesh is obtained through 3 mesh adaptions. The mesh topology of the busbar compartment at 10mm from the enclosure is

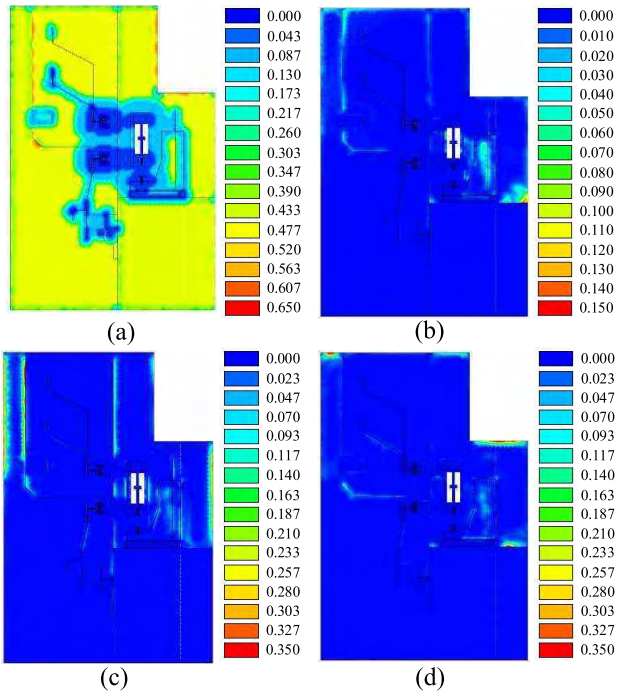

FIGURE 6. Error index distribution of the initial mesh. (a) Error index of T. (b) Error index of v_x. (c) Error index of v_y (d) Error index of v_z.

TABLE 1. Mesh adaption results.

Method	Adaption No.	Error index	N	T_{max}/°C	△
Initial	0	v_x v_y v_z	5657146	89.1	-
Posterior error estimation	1	v_x v_y v_z	7159444	66.9	24.9%
	2	v_x v_y v_z	8891692	71.1	6.3%
	3	T	10712838	68.3	3.9%
Global refining	1	-	9948593	77.0	13.6%
	2	-	17124637	71.3	7.4%
	3	-	33198736	69.5	2.5%

shown in Fig.7. Table 1 also shows the change of maximum temperature T_{max} and the total number of elements N of each mesh generation, in comparison with that obtained by the traditional global-refining method. The difference of the final T_{max} of the two methods is 1.2 °C, indicating their consistency in the reducing the numerical error. But the total elements of the final mesh based posterior error estimation is only 32.3% of that based on the tradition method. So the mesh size is significantly reduced and the adaption process is accelerated.

IV. BOUNDARY CONDITIONS

A. CONVECTIVE HEAT TRANSFER COEFFICIENT OF THE ENCLOSURE

1) EXTERNAL FLOW MODEL OF SWITCHGEAR

An external flow model of switchgear is built to calculate the convective HTC h_c under natural convection and forced convection environment. As shown in Fig.8, The model is

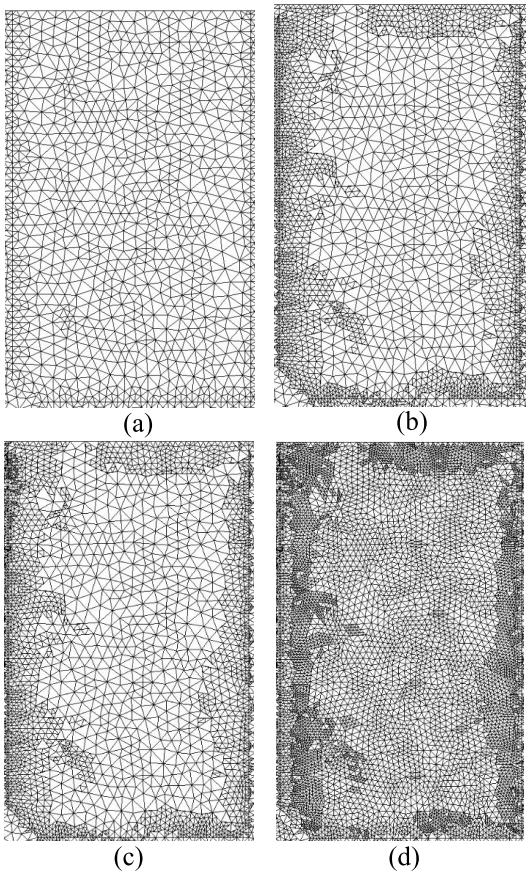

FIGURE 7. Mesh generated based on posterior error estimation. (a) Initial mesh. (b) Adaption 1. (c) Adaption 2. (d) Adaption 3.

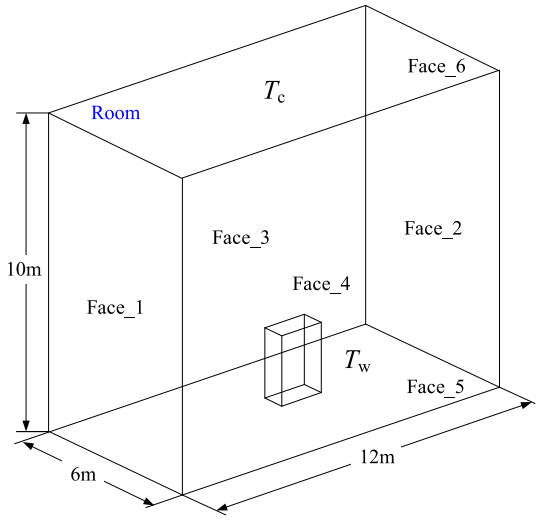

FIGURE 8. External flow calculation model of switchgear.

enclosed with the outer wall of the room and the switchgear enclosure is the inner boundary.

The temperature on the same board of the enclosure is thought to be the same. Then temperature T_w of each board are applied as the inner boundary condition respectively and the outer boundary condition varies according the convection environment.

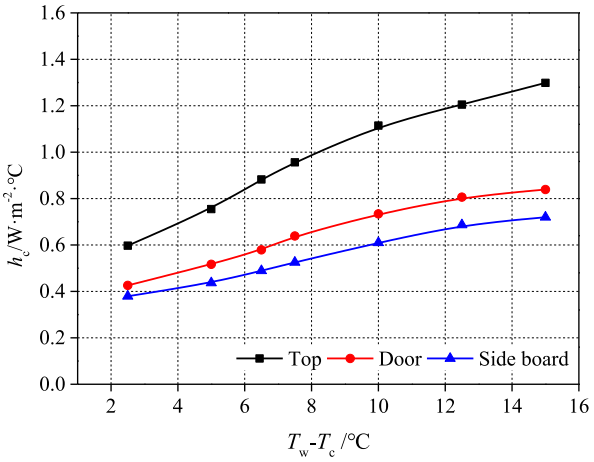

FIGURE 9. Simulation results of convective heat transfer coefficient (T_c = 25 °C).

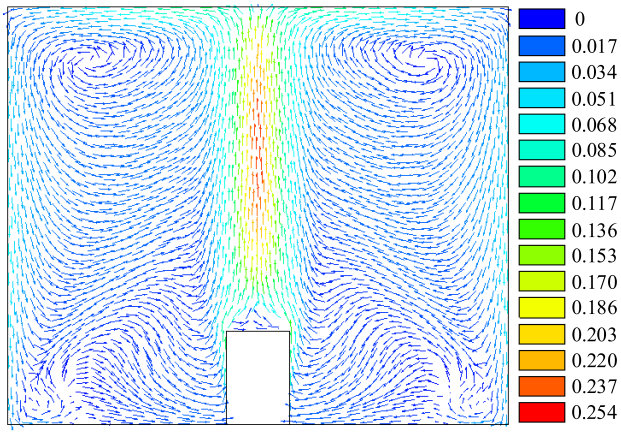

FIGURE 10. Air velocity distribution of the external flow model (m/s).

The external flow field and thermal field are solved according to (2) ∼ (4) and the average convective heat flux q_w of each board are derived. The corresponding convective HTC h_c under ambient temperature T_c are calculated with (7).

2) CONVECTIVE HEAT TRANSFER COEFFICIENT H_C UNDER NATURAL CONVECTION ENVIRONMENT

The external convection is mainly induced by the heating effect of switchgear while no additional ventilation equipment is installed,. Ambient temperature T_c are applied to the outer boundary of the model as its temperature is almost unaffected considering the room size.

The relationship between h_c and temperature difference (T_w-T_c) when T_c = 25 °C is shown in Fig.9. Results show that h_c changes along with the temperature difference (T_w-T_c) and the wall orientation. Coefficient h_c increases when the rise of the enclosure temperature strengthens the convection near switchgear. The coefficient h_c at the top of the switchgear is always higher than that of the side boards and doors. Because air velocity above the switchgear is much higher according to the sectional velocity distribution in Fig.10.

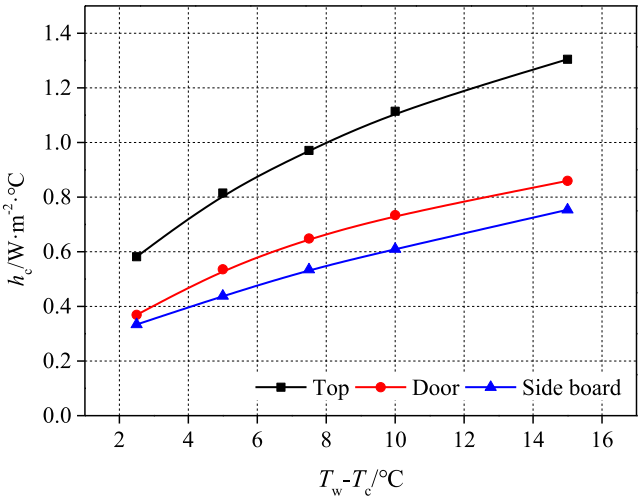

FIGURE 11. Convective heat transfer coefficient under different ambient temperature.

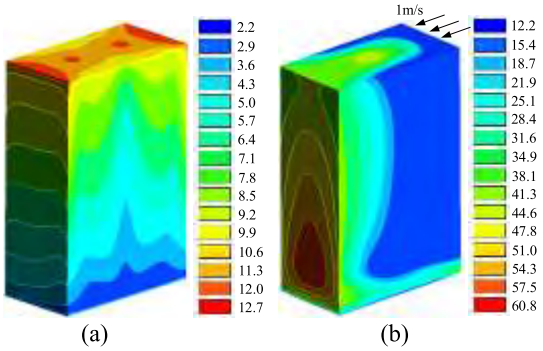

FIGURE 12. Convective heat flux under distribution under natural convection and forced convection environment (W/m^2). (a) Natural convection. (b) Forced convection.

Convective HTC h_c under different ambient temperature is shown in Fig.11 and the inner wall temperature T_c is fixed at 35 °C. The relationship between h_c and (T_w-T_c) is basically the same as that in Fig.9. By the results in Fig.9 and Fig.11, the range of convective HTC h_c under natural convection (no wind condition) is 0.4 W/(m^2 · °C) ∼ 1.4 W/(m^2 · °C), which is much smaller than the empirical values.

In order to validate the simulated h_c in Fig.9 and Fig.11, the results are compared with that computed with the empirical formulas. Taking $g = 9.8$ m/s^2, $\beta = 3.3 \times 10^{-3}$ °C^{-1}, $\theta = 15.0$ °C, $L = 9.0$ m, $\mu = 1.8 \times 10^{-5}$ kg/(m · s), $\rho = 1.2$ kg/m^3, $c_p = 1.0 \times 10^3$ J/(kg·°C), $\lambda = 2.6 \times 10^{-2}$ W/(m·°C) according to the final simulation results in Section V, the h_c calculated with (11) ∼ (13) is 1.7 W/(m^2 · °C). It is of the same scale with the one in Fig.9 and Fig.10, verifying the validity of the results.

In fact, the temperature and heat flux on a single board is different (Fig.12 (a)). Area weighted mean temperature of is taken as the temperature T_w instead to describe the average convective effect. Iterative method is also needed during calculation as the h_c is the function of T_w.

TABLE 2. Heat generation of different components (three phase).

Component	DC /W	50Hz /W	△	Volume /cm^3
Vacuum Interrupter	18.54	19.47	5.02%	309
Clubs contactor (Busbar compartment)	0.96	1.23	28.13%	426
Clubs contactor (Cable compartment)	0.96	1.23	28.13%	426
Busbar	85.44	93.22	9.11%	2177
Outlet and contact arm	11.7	16.77	43.33%	4127
Sum	117.6	131.92	12.18%	7465

3) CONVECTIVE HEAT FLUX UNDER FORCED CONVECTION ENVIRONMENT

Forced convection is simulated by making Face_1 and Face_2 in Fig.8 the inlet and outlet respectively. When 25 °C airflow with velocity 1 m/s entries the room from Face_2, normally, the convective heat flux distribution on the enclosure is shown in Fig.12 (b). Results show that the convective heat flux under forced convection environment is far more non-uniform due to the turbulence development near the enclosure. Thus, distributed convective h_c should be defined instead of the area weighted one under natural convection environment in section.A.2. Coupled calculation between the internal and the external flow field is a more accurate way to consider the effect of forced convection environment.

B. RADIATIVE HEAT TRANSFER

Taking the emissivity of the steel as $\varepsilon_1 = 0.1$ considering its polished surface and the ambient temperature $T_c = 25$ °C, the radiative heat flux at the enclousure under rated working condition is shown in Fig.13. The total radiative heat power reaches 47.7W. Thus, it's also necessary to take the influence of radiation into consideration in the thermal-fluid calculation.

V. HEAT GENERATION IN SWITCHGEAR

A. HEAT SOURCE DISTRIBUTION

Eddy current field is used to solve the heat source distribution in this section. The governing equations are [17]

$$\nabla \times \frac{1}{\mu}(\nabla \times \boldsymbol{A}) = -\frac{1}{\rho_e}\frac{\partial \boldsymbol{A}}{\partial t} - \frac{1}{\rho_e}\nabla V \tag{19}$$

$$\nabla \cdot \boldsymbol{A} = 0. \tag{20}$$

where $\boldsymbol{A}$ is the magnetic vector potential; V is the scalar potential; ρ_e is the resistivity;

The heat generation comparison between DC condition and power-frequency condition is shown in Table 2. The total heat generation increases 12.18% under 50 Hz due to the current uniformity caused by the proximity effect and the skin effect.

The eddy losses at the enclosure and the clapboards is shown in Fig.14. The total eddy losses in the clapboards is 40W, which is mainly induced near the contact boxes. The total eddy losses is 18W in the enclosure, which mainly concentrates in the side board near the incoming busbar.

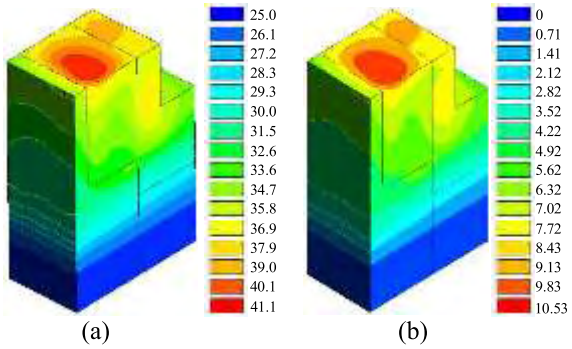

FIGURE 13. Temperature and radiative power distribution of the shell. (a) Temperature distribution (°C). (b) Convective heat flux (W/m^2).

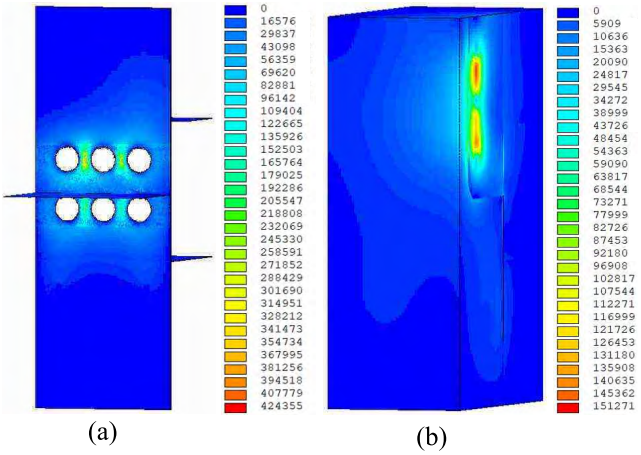

FIGURE 14. Distribution of eddy current loss (W/m^3). (a) Baffle. (b) Enclousure.

The eddy losses in the grounding switch can be ignored as it is as small as 1W.

Contact heat sources are calculated with the Ohm's Law. The measured total contact resistance of the contacts in circuit breaker for the A, B, and C phase are 93.6 $\mu\Omega$, 87 $\mu\Omega$, and 96 $\mu\Omega$ respectively. The average contact resistance of bolt structure is 4.2 $\mu\Omega$.

$$Q_c = I^2 R_c \tag{21}$$

where Q_c is the contact heat source; I is the root mean square (RMS) value of current; R_c is the contact resistance.

B. INFLUENCE OF HEAT SOURCE ON THE THERMAL FIELD

Bulk Joule losses, contact heat sources, and eddy losses are coupled to the thermal-fluid field of switchgear and their influence are researched in this section. Thermal filed under four combinations of heat source are compared in Fig.15: (a) DC bulk Joule losses; (b) 50Hz bulk Joule losses; (c) 50Hz bulk Joule losses and contact heat sources; (d) 50Hz bulk Joule losses, contact heat sources, and eddy losses. The rated current I = 630A is applied and the ambient temperature $T_c = 25$ °C.

Maximum temperature in Fig.15 (a) ~ Fig.15 (d) increase by 12.05%, 64.94% and 4.59% respectively, indicating that the degree of influence is: contact heat sources > frequency

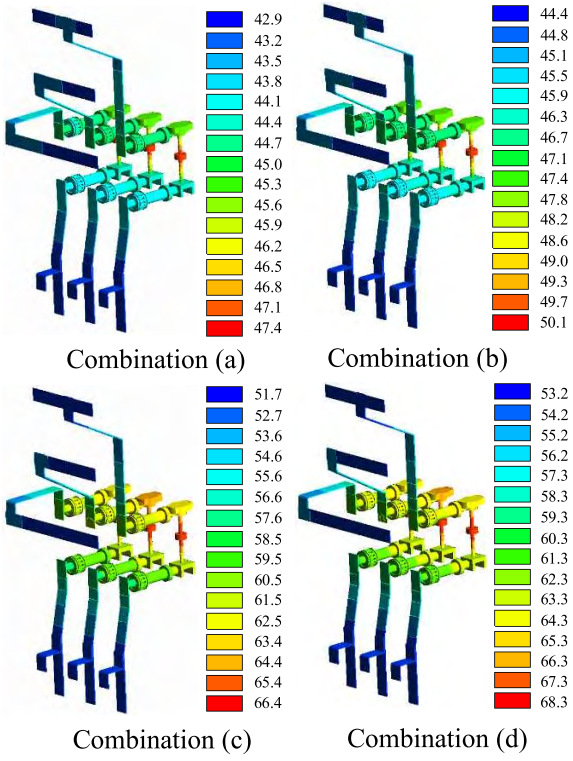

FIGURE 15. Influence of heat source on the thermal field (°C).

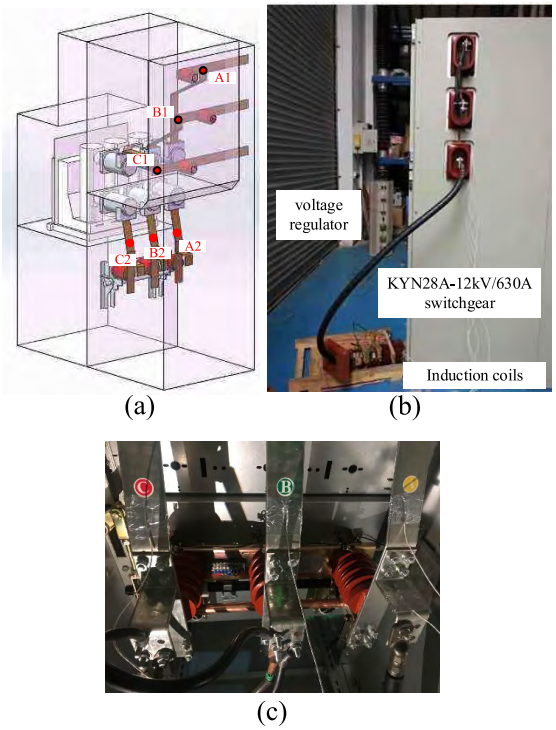

FIGURE 16. Steady-state temperature rise test of switchgear. (a) Measure points. (b) Test arrangement. (c) Thermocouples.

effect > eddy current loss. To improvement the simulation accuracy, the mentioned heat sources should be fully considered.

TABLE 3. Comparison of simulation and test results.

Point	T_c/°C	T_t/°C	Δ
A1	53.2	55.0	3.33%
A2	59.2	61.2	3.34%
B1	55.8	56.7	1.62%
B2	58.9	61.0	3.43%
C1	56.1	57.3	2.01%
C2	58.8	60.3	2.50%

VI. TEST VERIFICATION

The optimization methods of grid control, boundary conditions, and heat sources are applied to the thermal-fluid numerical calculation of the switchgear. The temperature distribution of the main circuit is shown in Fig.15(d). Steady temperature rise test is carried out to verify the validity of the simulation results. As shown in Fig.16, K-type thermocouples are mounted on the solid surface of busbars with aluminum foil. The uncertainty of the thermocouples is within 1.5 °C. Comparison between calculated results and measured datas is shown in Table 3. The maximum relative error is 3.43%, illustrating the effectiveness of the proposed methods.

VII. CONCLUSION

This paper studies the optimization methods for thermal-fluid numerical calculation of switchgear from mesh control, boundary condition, and heat sources.

Posterior error estimation guides the mesh adaption so that the process of mesh generation is accelerated and mesh redundancy is reduced. However the element proportion to be refined and the convergence criterion is still determined artificially. Supplementary researches on control parameters are still needed to further improve the efficiency of mesh adaption.

External flow model is built to determine the convective heat transfer coefficient h_c of the enclosure under natural convection environment, replacing the empirical values. The model can be can be extended to more complex operating environments.

Electromagnetic-thermal-fluid coupled calculation is applied to study the influence of different heat source. Bulk Joule losses, contact heat sources, and eddy losses should be fully considered in thermal field calculation of switchgear.

The proposed method and reference results can improve the efficiency and accuracy of thermal-fluid numerical calculation of switchgear, providing more accurate data support for heat dissipation analysis and design of switchgear.

REFERENCES

[1] H. Lü, L. Wang, W. Zheng, L. Wang, and J. Lin, "Coupled simulation of eddy-current thermal field in medium voltage switchgear," in *Proc. 3rd ICEPE-ST*, Busan, Korea, 2015, pp. 63–68.

[2] S. Sun, L.-A. Chen, Y.-M. You, and Z.-X. Ma, "Thermal analysis of switchgear using FEM considering the heat from the main circuit," in *Proc. 4th ICEPE-ST*, Xi'an, China, 2017, pp. 707–710.

[3] M. Li, X. Li, J. Lin, and L. Wang, "Temperature rise characteristics simulation of 40.5 kV high current cubicle type gas insulated switchgear," in *Proc. 1st ICEMPE*, Xi'an, China, 2017, pp. 616–619.

[4] L. Wang, W. Zheng, L. Wang, J. Lin, X. Li, and S. Jia, "Electromagnetic-thermal-flow field coupling simulation of 12-kV medium-voltage switchgear," *IEEE Trans. Compon., Packag., Manuf. Technol.*, vol. 6, no. 8, pp. 1208–1220, Aug. 2016.

[5] E. Fjeld, W. Rondeel, K. Vaagsaether, and E. Attar, "Influence of heat source location on air temperatures in sealed MV switchgear," in *Proc. 24th CIRED*, Glasgow, U.K., 2017, pp. 233–237.

[6] M. Bedkowski, J. Smolka, A. Ryfa, Z. Bulinski, and A. J. Nowak, "Heat dissipation within electrical switchgear enclosure," in *Proc. CEM*, London, U.K., 2014, pp. 1–2.

[7] S. Siddiqa, M. A. Hossain, and S. C. Saha, "The effect of thermal radiation on the natural convection boundary layer flow over a wavy horizontal surface," *Int. J. Therm. Sci.*, vol. 84, pp. 143–150, Oct. 2014.

[8] A. K. Sharma, K. Velusamy, C. Balaji, and S. P. Venkateshan, "Conjugate turbulent natural convection with surface radiation in air filled rectangular enclosures," *Int. J. Heat Mass Transf.*, vol. 50, nos. 3–4, pp. 625–639, Feb. 2007.

[9] G. Lauriat and G. Desrayaud, "Effect of surface radiation on conjugate natural convection in partially open enclosures," *Int. J. Therm. Sci.*, vol. 45, no. 4, pp. 335–346, Apr. 2006.

[10] M. Bedkowski *et al.*, "Coupled numerical modelling of power loss generation in busbar system of low-voltage switchgear," *Int. J. Therm. Sci.*, vol. 82, pp. 122–129, Aug. 2014.

[11] M. Bedkowski, J. Smolka, Z. Bulinski, A. Ryfa, and M. Ligeza, "Experimentally validated model of coupled thermal processes in a laboratory switchgear," *IET Gener. Transmiss. Distrib.*, vol. 10, no. 11, pp. 2699–2709, Apr. 2016.

[12] M. Bedlkowski, J. Smolka, Z. Bulinski, and A. Ryfa, "Simulation of cooling enhancement in industrial low-voltage switchgear using validated coupled CFD-EMAG model," *Int. J. Therm. Sci.*, vol. 111, pp. 437–449, Jan. 2017.

[13] E. Fjeld, W. Rondeel, S. T. Hagen, and M. Saxegaard, "Estimating the temperature rise of load break switch contacts in enclosed MV switchgear," in *Proc. 24th CIRED*, Glasgow, U.K., 2017, pp. 136–139.

[14] Y. A. Cengel, "Fundamentals of convection," in *Heat and Mass Transfer: A Practical Approach*, 3rd ed. New York, NY, USA: McGraw-Hill, 2006, ch. 6, sec. 1, pp. 334–336.

[15] B. E. Launder and D. B. Spalding, "The numerical computation of turbulent flows," *Comput. Methods Appl. Mech. Eng.*, vol. 3, no. 2, pp. 269–289, 1974.

[16] J. Dannenhoffer and J. Baron, "Grid adaptation for the 2-D Euler equations," in *Proc. 23rd ASM*, New York, USA, 1985, pp. 1–11.

[17] C. Liu, J. Ruan, W. Wen, R. Gong, and C. Liao, "Temperature rise of a dry-type transformer with quasi-3D coupled-field method," *IET Electr. Power App.*, vol. 10, no. 7, pp. 598–603, Jul. 2016.

JIANGJUN RUAN was born in Zhejiang, China, in 1968. He received the B.S. and Ph.D. degrees in electric machine engineering from the Huazhong University of Science and Technology, Wuhan, China, in 1990 and 1995, respectively. He was a Postdoctoral Researcher with the Wuhan University of Hydraulic and Electric Engineering, Wuhan, in 1998.

He is currently a Professor with the School of Electrical Engineering, Wuhan University. His research interests include electromagnetic field numerical simulation, and high voltage and insulation technology.

YONGCONG WU was born in Guangdong, China, in 1991. He received the B.S. degree in electrification and automation from the School of Electrical Engineering, Wuhan University, Wuhan, China, in 2013, where he is currently pursuing the Ph.D. degree.

His research interests include high voltage apparatus and external insulation of transmission line.

PENG LI was born in Hubei, China, in 1989. He received the B.S. degree in electrification and automation from the School of Electrical and Information, Northeast Agricultural University, Harbin, China, in 2012, and the Ph.D. degree in high voltage and insulation technology from the School of Electrical Engineering, Wuhan University, Wuhan, China, in 2018.

He is currently a Lecturer with the College of Electrical Engineering and New Energy, China Three Gorges University, Yichang, China. His research interests include external insulation of transmission line, high voltage apparatus, and multi-physics analysis of electrical equipment.

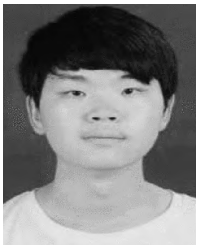

MINGYANG LONG was born in Henan, China, in 1992. He received the B.S. degree in electrical engineering and automation from the School of Electrical Engineering, Wuhan University, Wuhan, China, in 2015, where he is currently pursuing the M.S. degree.

His research interests include high voltage and insulation technology.

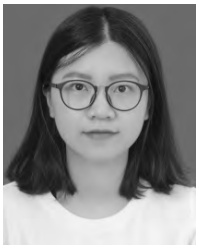

YUJIA GONG was born in Hubei, China, in 1995. She is currently pursuing the M.A. degree with the School of Electrical Engineering and Automation, Wuhan University, Wuhan, China.

Her current research interest includes electromagnetic launch technology and its applications.